Laminar Flow of Four Gases Through a Helical Rectangular Duct

Robert F. Berg and Stuart A. Tison
Process Measurements Division, National Institute of Standards and Technology, Gaithersburg, MD 20899

Measurements and a model of gas flow through a helical duct of rectangular cross section are reported. Observations of the rate of rise of pressure in a known volume located downstream from the duct yielded molar flow rates of helium, nitrogen, argon and sulfur hexafluoride. The model predicts flow rates from the duct's entrance pressure, exit pressure, and temperature. It accounts for the gas's nonideal equation of state, gas expansion along the duct's length, the increase of kinetic energy near duct's entrance, and slip. After adjusting only one parameter (the duct's height), the model agrees with the data to within 0.2% in the range of Reynolds number $0.08 < Re < 40$. To extend the model to $Re = 1{,}000$, the centrifugal effects were accounted for by rescaling Targett et al.'s (1995) numerical calculations. The extended model agrees with the data to within 0.2% in the range $40 < Re < 400$ and to within 1% in the range $400 < Re < 1{,}000$.

Introduction

An accurate hydrodynamic model of flow through a duct allows the duct to serve as either a viscometer or as a flowmeter. The model yields viscosity from measurements of the duct's entrance and exit pressures if the flow rate is known. Conversely, the model yields the flow rate if the fluid's viscosity is known. The effective radius of the duct is usually determined by calibration with a fluid of known viscosity at a known flow rate.

The present work is directed toward understanding the flow of gas through a duct with an accuracy sufficient to allow the duct to be used as a flow transfer standard for a variety of gases. This requires a hydrodynamic model with an accuracy of approximately 0.1%. Here we describe measurements and a model of the flow rates of four gases through a laminar flow element (LFE) consisting of a helical duct of rectangular cross section. The measurements yielded molar flow rates $\dot{n}$ from observations of the rate of rise of pressure in a known volume located downstream from the duct. The model yielded flow rates $\dot{n}_{\text{model}}$ based on the gas properties and the entrance pressure, exit pressure, and temperature of the duct. Figure 1 compares the model to the measurements by displaying the ratio $\dot{n}/\dot{n}_{\text{model}}$ as a function of Reynolds number Re. In the range $0.08 < Re < 40$, virtually all of the data lie within 0.2% of the model. The agreement between the model and the data required only one adjustable parameter, the duct's height, and the agreement among the four gases required none. This consistency demonstrates simultaneously the reliability of both the measurements and the model.

The model corrects the Poiseuille description for kinetic energy changes at the duct's entrance, gas expansion along the duct's length, the effects of slip, and the gas's nonideal equation of state. Making the duct's length much longer than its effective radius reduced the size of the first two corrections. We coiled the 3-m-long duct into a regular helix to fit it into a small thermostatted volume.

The duct's helical curvature introduced centrifugal effects that became very large for flow rates that exceeded the critical Dean number Dn_c. These effects required an extension to the model with the form $\dot{n}_{\text{model}} f_c(Dn)$. Here the function $f_c(Dn)$ depends on the Dean number, defined here as

$$Dn \equiv Re\left(\frac{2b}{R_{\text{helix}}}\right)^{1/2}, \tag{1}$$

where $2b$ and R_{helix} are the duct's height and the helix's radius of curvature, respectively. In the limit where the duct's height-to-width aspect ratio b/a approaches zero, centrifugal

Correspondence concerning this article should be addressed to R. F. Berg.
Present address of S. A. Tison: Millipore Corporation, 915 Enterprise Boulevard, Allen, TX 75013.

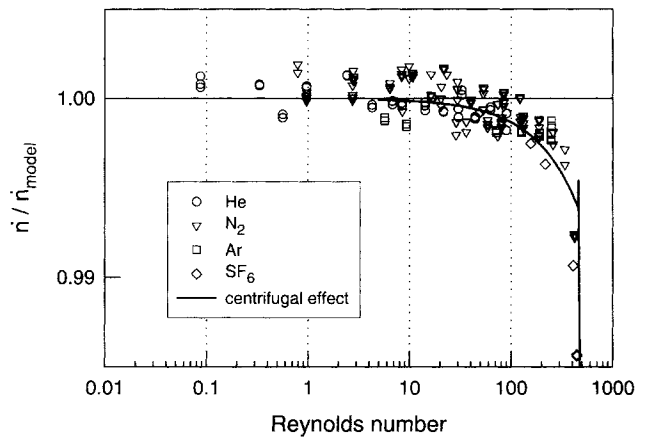

Figure 1. Measured molar flow rates $\dot{n}$ divided by modeled flow rates $\dot{n}_{model}$ as a function of Reynolds number.

The model's only free parameter was the duct's height b. The data below $Re = 40$ agree with the model to within their scatter and the uncertainties of the viscosity ratios. The data in the range $40 < Re < 400$ agree with the extended model $\dot{n}_{model} f_c$ that includes centrifugal effects.

effects are predicted to occur only above the critical value $Dn_c = 35.9$ (Dean, 1928; Walowit et al., 1964). The data near Dn_c in Figure 2 have a sharp change of slope consistent with this prediction. The data above Dn_c agree with the extended model, which we obtained by rescaling Targett et al.'s (1995) numerical calculations by a second adjustable parameter. Targett et al.'s calculations also predicted small centrifugal effects *below* Dn_c due to the duct's finite width. The agreement of the extended model with the data below Dn_c in Figure 1 supports this prediction. Thus, by including centrifugal effects, the extended model is valid up to $Re = 400$. More generally, a numerical calculation of centrifugal effects appears to be both necessary and sufficient for accurately modeling similar ducts at Dean numbers up to $0.8Dn_c$.

The present model is more accurate than previous models of flowmeters because, in addition to the more common corrections used by others, it includes an accurate correction for gas expansion based on the work of van den Berg et al. (1993a). This accuracy eliminated the need for an adjustable term proportional to Re frequently used in more empirical models. As a consequence, the presence of centrifugal effects at Dean numbers below Dn_c, which were also proportional to Re in the present duct, could be demonstrated for the first time.

The model is useful because it can be extended from a rectangular cross section to a different shape, such as a circle or an annulus. The model is useful also because it is easily understood. The corrections enter the model linearly, so that the relative importance of slip, for example, is simply the size of the slip term. The corrections are expressed in terms of familiar dimensionless parameters such as the Reynolds number.

Previous work

Models that include some of the phenomena considered here have been devised to correlate the performances of flow impedances used in flowmeters, heat exchangers, and pneumatic instrumentation. For example, Ruegg and Allion (1966) used various approximations to solve a generalized flow equation that they attributed to Shapiro (1953). Their analysis assumed an ideal gas without slip, but included entrance, exit, and heat-loss effects. The standard deviation of the fit to their data for helium and air was 0.4%. The model used by Lee et al. (1971) is similar to that used here, but it assumed an ideal gas without corrections for nonideality and slip. To within 3%, it described flow data where the exit/entrance pressure ratio was as small as 0.5. Delajoud and Girard (1994) described the calibration of a commercial flowmeter based on an annular flow impedance. They explicitly included the gas's nonideality, and they modeled other corrections as a function of Re. This function, which was obtained by calibration, was gas-dependent and apparently empirical.

More accurate models have been used to describe capillary viscometers of circular cross section. For example, Flynn et al. (1963) and Dawe and Smith (1970) used similar models that applied corrections for slip, the entrance effect, and gas nonideality. Van den Berg et al. (1993a) constructed the most careful model of isothermal flow through a capillary of circular cross section. Starting with the conservation equations for mass, momentum, and energy, they derived a differential equation for the radial-velocity profile. They obtained solutions to this equation in both analytic perturbation form and numerical form. They justified the isothermal assumption in a separate article (Van den Berg et al., 1993b).

Most studies of centrifugal effects have involved flow through ducts of circular cross section. Reviews have been written by White (1929), Ito (1959, 1987), and Berger et al. (1983). Dawe (1973) experimentally studied the effect of the coiled capillary's curvature. His result for Dn_c was 0.6 times the value predicted for a duct of circular cross section, perhaps because his method relied on a time-dependent flow

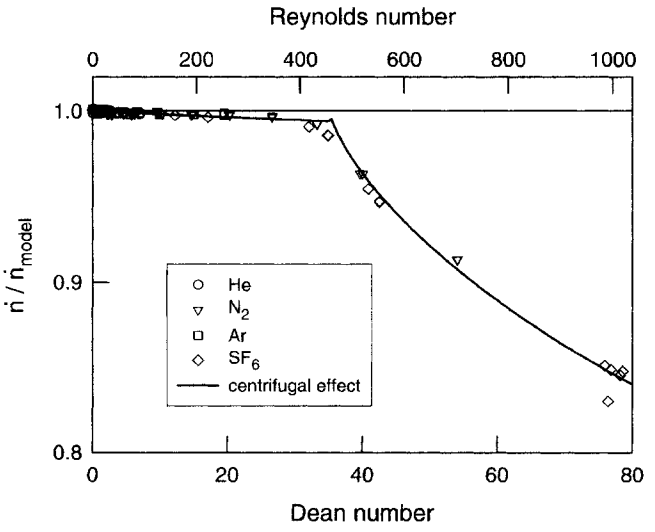

Figure 2. Measured molar flow rates $\dot{n}$ divided by modeled flow rates $\dot{n}_{model}$ as a function of Dean number.

The extended model $\dot{n}_{model} f_c$ that includes centrifugal effects was obtained by rescaling the numerical calculations of Targett et al. (1995) to fit the data near $Dn = 80$.

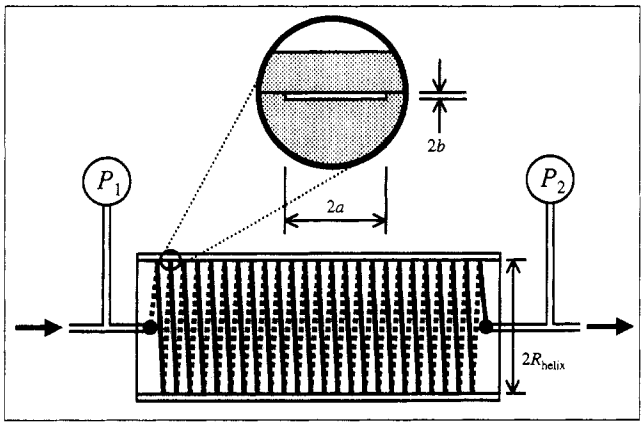

Figure 3. Laminar flow element constructed by machining a helical, rectangular channel onto a stainless-steel rod and shrink-fitting the rod into a matching cylinder.

The height of the duct's rectangular cross section was $2b$ = 0.1 mm, and the aspect ratio was approximately $b/a = 1/15$.

rate. Targett et al. (1995) give a recent summary of measurements and calculations for rectangular cross sections. There have been no accurate measurements of the flow impedance of curved rectangular channels of narrow aspect ratio ($b/a \ll 1$).

Experimental Apparatus and Method

Laminar flow impedance

Figure 3 shows the geometry of the LFE. The duct was constructed by machining a shallow rectangular channel onto a stainless-steel rod. The channel followed a helical path in the manner of a screw thread. Shrink fitting the rod into a matching stainless-steel cylinder covered the channel to create a helical duct of rectangular cross section. This construction made the LFE especially stable against changes in geometry. Fittings were welded onto the cylinder to connect the LFE to external plumbing. Table 1 gives the duct's measured dimensions.

The inlet pressure P_1 and outlet pressure P_2 were measured by separate transducers having full-scale ranges of 1.4 MPa and 0.3 MPa, respectively. The uncertainty of the pressure measurements was 0.01% of the full-scale values. The LFE's temperature T was measured by a platinum resistance thermometer. The LFE and the pressure transducers were contained in a stirred air bath maintained constant to within 0.02 K at a temperature near 25°C. More details are in the article by Tison and Berndt (1997).

The duct's small height and long length gave the LFE three important advantages for use as a gas-flow transfer standard.

Table 1. Dimensions of the Helical Duct

Width	2a	1.59 ± 0.03 mm
Height	$2b$	102 ± 5 μm
Length	L	3.2 ± 0.1 m
Inner radius	R_{helix}	17.18 ± 0.01 mm
Thread pitch		2.50 mm

First, even a small flow created a pressure difference large enough to be accurately measured. For example, at the lowest flow rate reported here, the pressure difference $P_1 - P_2$ was approximately 6 kPa. The relative uncertainty of the best primary standards at this pressure is approximately 10^{-5} (Miiller, private communication, 1999). Second, the small value of the length ratio b/L minimized the uncertainty associated with the pressure drops near the entrance and exit. Third, the small height-to-width aspect ratio, $b/a \ll 1$, minimized centrifugal effects below the critical Dean number.

Constant-volume flowmeter

The flows were measured with a constant-volume (pressure rate-of-rise) flowmeter consisting of a 153-L vacuum chamber, a 1.4-L side volume, and attached pressure and temperature gauges. The chamber's volume was determined to within 0.03% by expanding nitrogen gas from a calibrated volume into the vacuum chamber. The side volume was determined similarly. The average temperature T of the volume used to measure the flow rate was determined from the weighted average of platinum resistance thermometers attached to the volume's exterior. The temperature uncertainty was approximately 0.06 K and was dominated by temperature gradients across the volume. Capacitance diaphragm gauges measured the pressure P in the vacuum chamber below 1.3 kPa. At higher pressures, a quartz Bourdon tube gauge was used. The flowmeter's standard uncertainty was approximately 0.1% throughout the range of flows reported here.

Flow-rate measurements

The LFE's entrance was attached to a gas supply regulated at pressure P_1, and its exit was attached to a variable leak valve. When necessary, this valve was adjusted between measurements to keep P_2 within 10% of 105 kPa. Gas exiting the LFE via the variable leak valve entered the evacuated constant-volume flowmeter, whose pressure and temperatures were periodically recorded. The only data analyzed were those recorded after the LFE's pressure difference $P_1 - P_2$ and the constant-volume flowmeter's rate of rise $\dot{P}$ had stabilized. The molar flow rate into the constant-volume flowmeter was calculated from the pressure rate-of-rise as

$$\dot{n} = \frac{\dot{P}V}{RT}, \tag{2}$$

where V is the constant-volume flowmeter's volume and R is the universal gas constant. Virial corrections were unnecessary at the low pressures used in the constant-volume flowmeter.

Figure 4 shows the range of $\dot{n}$ spanned by the approximately 170 measurements made with helium, nitrogen, argon, and sulfur hexafluoride. These gases, which are relatively inert, allowed us to vary the molecular weight by a factor of 36 and the pressure virial coefficient by a factor of 55.

Analysis

Model

The LFE's impedance was approximately that of an ideal rectangular duct. The volume flow rate of an *incompressible*

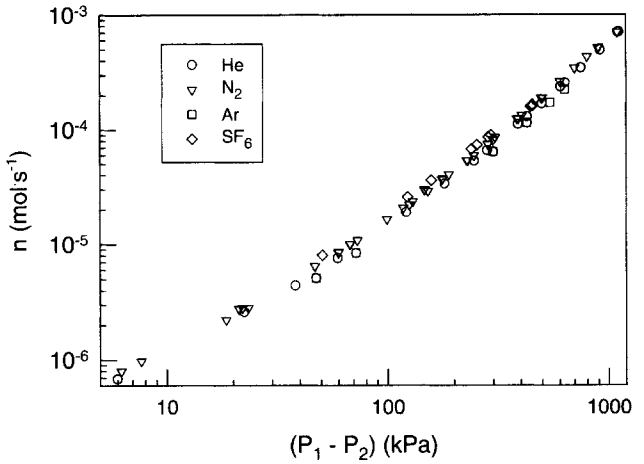

Figure 4. Molar flow rates as a function of LFE's pressure difference $P_1 - P_2$.

A variable leak valve kept the exit pressure P_2 within 10% of 105 kPa.

fluid through such a duct is

$$Q_0 = \frac{4F_p ab^3(P_1 - P_2)}{3\eta L}, \tag{3}$$

where η is the fluid's viscosity. The dimensionless shape factor F_p depends only on the aspect ratio b/a (Carley, 1958). In the limit $b/a \ll 1$, $F_p \cong 1$ because the flow profile approaches the profile between infinite parallel plates. The present LFE was close to this limit: the value of b fitted to Eq. 4 below led to $F_p \cong 0.96$.

As described in Appendix A, we generalized Eq. 3 to a compressible fluid and obtained the modeled flow rate

$$\dot{n}_{\text{model}} = \left[\left(\frac{P_1 Q_0}{RT}\right)\left(\frac{1+y}{2}\right)\right]\left[1 + g_{\text{virial}}(B_P P_1, y) + \frac{K_{\text{ent}}}{6}\frac{b}{L}Re + \frac{K_{\text{exp}}}{5}\frac{b}{L}Re\ln(y) + 6K_{\text{slip}}Kn\right], \tag{4}$$

where B_P is the gas's second pressure virial coefficient and $y \equiv P_2/P_1$ is the ratio of exit pressure to entrance pressure. The factor $(1+y)/2$ is proportional to the average of P_1 and P_2, and it accounts for the average density being lower than the entrance density. It was as small as 0.55 for the largest pressure drops.

The second bracket of Eq. 4 contains four dimensionless correction terms, which are functions of the pressure ratios $B_P P_1$ and y, the length ratio b/L, the Reynolds number Re, and the Knudsen number Kn. The first term corrects for deviations from ideal-gas compressibility. A deviation that increases the average density increases the flow rate. The second term corrects for the increase of kinetic energy that occurs near the duct's entrance. The increase occurs because the gas's average velocity increases as it flows into the mouth of the duct. It increases further as the flow profile changes from nearly uniform at the entrance to nearly parabolic farther downstream. The resulting pressure drop decreases the flow rate. The third term corrects for gas expansion along the duct, which also increases the kinetic energy and decreases the flow rate. The fourth term corrects for slip at the duct's walls. Slip increases the flow rate.

The viscosity used in Eq. 4 is the value averaged along the length of the duct

$$\bar{\eta} \equiv \frac{1}{L}\int_0^L \eta(z)\,dz \cong \eta(T, \bar{P}), \tag{5}$$

where z is the axial position along the length of the duct. The average Knudsen number $Kn \equiv \bar{\lambda}/(2b)$ is defined in terms of the average mean free path

$$\bar{\lambda} \cong \frac{16}{5}\left(\frac{RT}{2\pi M}\right)^{1/2}\frac{\bar{\eta}}{\bar{P}}, \tag{6}$$

where M is the molar mass. In these definitions, the average pressure in the duct,

$$\bar{P} \equiv \frac{1}{L}\int_0^L P(z)\,dz = \frac{2}{3}\left(\frac{1+y+y^2}{1+y}\right)P_1, \tag{7}$$

was derived by neglecting the correction terms in Eq. 4.

Appendix A gives the function g_{virial} and the values of the coefficients K_{ent}, K_{exp}, and K_{slip}. Appendix B gives the gas property values used in the model.

Reynolds number definition

Two of the four corrections in Eq. 4 are functions of the Reynolds number, which is a local quantity that itself depends on z. In practice, this dependence is very weak because the dependence of the local density $\rho(z)$ cancels that of the local, radially averaged velocity $\langle v(z)\rangle$ according to

$$Re(z) = \frac{2b\langle v(z)\rangle\rho(z)}{\eta(z)} = \frac{M\dot{n}}{2a\eta(z)}. \tag{8}$$

The constant width $2a$ of the duct and the weak dependence of viscosity on density make $Re(z)$ a weak function of z. For example, for the largest flow rates of nitrogen through the LFE, the pressure decreased from $P_1 = 1$ MPa at the entrance to $P_2 = 0.1$ MPa at the exit, while $Re(z)$ increased by only 1%. We therefore defined the Reynolds number as

$$Re \equiv \frac{M\dot{n}}{2a\bar{\eta}}. \tag{9}$$

In Eq. 9, the value of $\dot{n}$ was estimated as $\dot{n}_{\text{model}}$ calculated without the Re-dependent correction terms of Eq. 4. The small size of these terms made iteration of Eq. 4 unnecessary.

Relative sizes of the corrections

Table 2 gives the maximum size of the correction terms in Eq. 4. Although three of the corrections were largest for SF_6

Table 2. Maximum Size of Correction Terms of Eq. 4

Effect	% of $\dot{n}$	Conditions
Nonideal gas equation of state	−4.5	SF_6 near $Re = 1{,}000$
Kinetic-energy increase near entrance	−0.3	SF_6 near $Re = 1{,}000$
Gas expansion along duct	−0.9	SF_6 near $Re = 1{,}000$
Slip	+1.0	He near $Re = 0.09$

at the highest flow rate, all four gases required at least two corrections exceeding 0.001 below $Re = 200$.

Results

Low flow rates

Figure 1 shows the accuracy of the modeled flow rates $\dot{n}_{\text{model}}$ by displaying the ratio $\dot{n}/\dot{n}_{\text{model}}$ as a function of Re. This agreement was obtained by adjusting the duct height $2b$ so that the points below $Re = 40$ lay near $\dot{n}/\dot{n}_{\text{model}} = 1$. The 5% uncertainty of the machined channel's depth made the adjustment necessary. Quite reasonably, the adjusted value $2b = (106.42 \pm 0.01)$ μm agrees with the height in Table 1.

For each gas, points differing from the gas's average value by more than three standard deviations were excluded. Virtually all of the remaining data lie within the band 1.000 ± 0.002 in the range $0.08 < Re < 40$. (At $Re = 40$, the nitrogen flow rate was $\dot{n} = 4.0 \times 10^{-5}$ mol·s^{-1}, or 54 standard cm^3 per minute.)

Centrifugal effects at high flow rates

Figure 2 shows that centrifugal effects caused large deviations of the data from the simple model $\dot{n}_{\text{model}}$ at high flow rates. This subsection describes an extended model with the form

$$\dot{n} = \dot{n}_{\text{model}}(Re) f_c\left(Dn, \frac{b}{a}, \frac{b}{R_{\text{helix}}}\right), \tag{10}$$

where the dimensionless function f_c depends on the Dean number and the two aspect ratios that characterize the duct's geometry. Because both aspect ratios were small ($b/R_{\text{helix}} \cong 0.0031$ and $b/a \cong 1/15$), we used the limiting value $Dn_c = 35.9$ that applies when both quantities approach zero. This is consistent with Walowit et al.'s (1964) calculations of Dn_c and the instability wavelength as a function of b/R_{helix}. However, as discussed below, the LFE's height-to-width aspect ratio b/a was large enough to affect f_c.

Below Dn_c, there have been no previous measurements of f_c. Numerical calculations by Targett et al. (1995) obtained the pressure drop of an incompressible liquid flowing around an annulus defined by two concentric cylinders of radii R_{helix} and $R_{\text{helix}} + 2b$. They calculated the pressure drop for $b/a = 0$ in the range $2 < Dn < 104$, and for $b/a = 1/16$, $1/12$, and $1/5$ in more limited ranges near Dn_c. For all four values of b/a, they used the value $b/R_{\text{helix}} = 0.025$. As predicted by Dean (1928), the values of f_c calculated for $b/a = 0$ were constant below Dn_c. In contrast, the values of f_c calculated for $b/a > 0$ depended on D_n because of secondary flow near the duct's corners. For the values of b/a that bracket the LFE's value (1/16 and 1/12), the deviations of f_c from unity were proportional to the product of b/a and Dn, specifically

$$f_c = f_- \equiv 1 - k_{\text{linear}}\left(\frac{b}{a}\right)\left(\frac{Dn}{Dn_0}\right), \quad Dn < Dn_c. \tag{11}$$

Here, Dn_0 is the adjustable parameter that Targett et al. used to describe their calculations above Dn_c. We divided Dn by Dn_0 to account for the dependence of f_c on b/R_{helix}, as described below. Fitting Eq. 11 to Targett et al.'s calculations below Dn_c yielded $k_{\text{linear}} = 0.60$.

Above Dn_c, there have been no previous measurements of f_c with $b/a \ll 1$. For the case $b/a = 0$, Targett et al. found that the empirical equation

$$f_c \cong f_+ \equiv \left[1 + \left(\frac{Dn - Dn_c}{Dn_0}\right)^{3/4}\right]^{2/3}, \quad Dn > Dn_c, \tag{12}$$

described their calculations to within 1% when they set $Dn_0 \equiv 130$. [The product of exponents in Eq. 12 has the asymptotic value 1/2 characteristic of a duct with a circular cross section at large Dn (Berger, 1983).]

We obtained the extended model f_c by rescaling Targett et al.'s calculations to match the present measurements. This required two assumptions about the form of f_c:

1. Above Dn_c, the empirical description f_+ that describes f_c for $b/a = 0$ is also valid for small, nonzero values of b/a. This allows f_c for the present measurements to be described by the combination

$$f_c \equiv \begin{Bmatrix} f_-, & Dn < Dn_c \\ f_+, & Dn > Dn_c \end{Bmatrix}. \tag{13}$$

(We did not include f_- as a term in f_+. This simplified the form of f_+ at the expense of a negligible discontinuity of f_c at Dn_c.)

2. Dn_0 is the only parameter that depends on b/R_{helix}.

These assumptions and the value of Dn_0 determined f_c above Dn_c. As shown in Figure 2, the choice $Dn_0 = 230$ causes the product $\dot{n}_{\text{model}} f_c$ to fit the data to within 1% over the range $Dn_c < Dn < 80$, corresponding to $456 < Re < 1016$. The remaining discrepancies are comparable to those between the calculated values and empirical description f_+ of Targett et al.

The same value of Dn_0 also determined f_c below Dn_c. As shown in Figure 1, $\dot{n}_{\text{model}} f_c$ describes the data to within 0.2% up to $Re = 400$, corresponding to $0.88 Dn_c$. In spite of this success, we did not incorporate f_c into the simple model because it relies on the preceding two assumptions and the second free parameter Dn_0. (The first is b.) We speculate that calculations similar to those of Targett et al. with the value of b/R_{helix} used here would yield a value of Dn_0 consistent with our data, thereby removing the need for these assumptions. Equation 4 could then incorporate f_c, thereby extending its range of validity up to $0.8 Dn_c$. The possibility of extending the model to Dean numbers above $0.8 Dn_c$ is less certain, because the secondary flow near Dn_c has a sensitive dependence on details of the duct's geometry.

Acknowledgments

This work was funded through the Office of Microelectronic Programs at NIST. Stuart Churchill and Arno Laesecke gave helpful information about flow through curved ducts. Jeff Kelley oversaw the construction of the LFEs.

Notation

a = duct half-width
b = duct half-height
B_P = pressure virial coefficient
Dn = Dean number
Dn_c = critical Dean number
$f_+ = f_c(Dn)$ for $Dn > Dn_c$
$f_- = f_c(Dn)$ for $Dn < Dn_c$
f_c = function accounting for centrifugal effects
f_s = accommodation coefficient
F_P = duct shape factor depending on b/a
g_{virial} = pressure virial correction
K_{ent} = entrance coefficient
K_{exp} = expansion coefficient
k_{linear} = coefficient for f_-'s dependence on Dn
K_{slip} = slip coefficient
Kn = Knudsen number
L = duct length
M = molecular mass
$\dot{n}$ = molar flow rate
P = pressure
$\overline{P}$ = average pressure
P_1 = pressure at entrance
P_2 = pressure at exit
Q_0 = volume flow rate for liquid Poiseuille flow
Q_1 = volume flow rate at duct entrance
R_{helix} = duct radius of curvature
Re = Reynolds number
T = temperature
v = velocity
$y = P_2/P_1$
z = axial coordinate along the helical duct

Greek letters

ΔP = pressure difference
η = viscosity
$\overline{\eta}$ = average viscosity
η_0 = viscosity at 25.00°C in limit of 0 Pa
κ = thermal conductivity
$\overline{\lambda}$ = average mean free path
ρ = density

Literature Cited

Batchelor, G. K., *An Introduction to Fluid Dynamics*, Sec. 5.15, Cambridge Univ. Press, Cambridge (1967).
Berger, S. A., L. Talbot, and L.-S. Yao, "Flow in Curved Pipes," *Ann. Rev. Fluid Mech.*, **15**, 461 (1983).
Bich, E., J. Millat, and E. Vogel, "The Viscosity and Thermal Conductivity of Pure Monatomic Gases from Their Normal Boiling Point up to 5000 K in the Limit of Zero Density and at 0.101325 MPa," *J. Phys. Chem. Ref. Data*, **19**, 1289 (1990).
Bich, E., and E. Vogel, "Initial Density Dependence," *Transport Properties of Fluids*, Chap. 5.2, J. Millat, J. H. Dymond, and C. A. Nieto de Castro, eds., Cambridge Univ. Press, Cambridge (1996).
Carley, J. F., and R. A. Strub, "Basic Concepts of Extrusion," *Ind. Eng. Chem.*, **45**, 970 (1953).
Dawe, R. A., and E. B. Smith, "Viscosities of the Inert Gases at High Temperatures," *J. Chem. Phys.*, **52**, 693 (1970).
Dawe, R. A., "A Method for Correcting Curved-Pipe Flow Effects Occurring in Coiled Capillary Viscometers," *Rev. Sci. Instrum.*, **44**, 1231 (1973).
Dean, W. R., "Fluid Motion in a Curved Channel," *Proc. Roy. Soc. Lond. A*, **121**, 402 (1928).
Delajoud, P., and M. Girard, "A High Accuracy, Portable Calibration Standard for Low Mass Flow," IMEKO World Congress of Metrology, Torino, Italy (1994).
Design Institute of Physical Property Data (DIPPR), Project 801, Thermophysical Properties Laboratory, Brigham Young University, Provo, UT 84602 (1999).
Dittmann, S., B. E. Lindenau, and C. R. Tilford, "The Molecular Drag Gauge as a Calibration Standard," *J. Vac. Sci. Technol. A*, **7**, 3356 (1989).
Flynn, G. P., R. V. Hanks, N. A. LeMaire, and J. Ross, "Viscosity of Nitrogen, Helium, Neon, and Argon from −78.5° to 100°C Below 200 Atmospheres," *J. Chem. Phys.*, **38**, 154 (1963).
Hoogland, J. H. B., H. R. van den Berg, and N. J. Trappeniers, "Measurements of the Viscosity of Sulfur Hexafluoride up to 100 bar by a Capillary-Flow Viscometer," *Physica*, **134A**, 169 (1985).
Ito, H., "Friction Factors for Turbulent Flow in Curved Pipes," *Rep. Inst. High Speed Mech.*, **11**, 1 (1959).
Ito, H., "Flow in Curved Pipes," *JSME Int. J.*, **30**, 262 (1987).
Kawata, M., K. Kurase, A. Nagashima, and K. Yoshida, "Capillary Viscometers," *Measurement of the Transport Properties of Fluids*, Chap. 3, W. A. Wakeham, A. Nagashima, and J. V. Sengers, eds., Blackwell, Oxford (1991).
Kestin, J., M. Sokolov, and W. Wakeham, "Theory of Capillary Viscometers," *Appl. Sci. Res.*, **27**, 241 (1973).
Lee, P. M., S. Lin, C. K. Kwok, and M. P. Du Plessis, "Similarity Rule for Design of Linear Fluid Resistors and Its Application for Flow Measuring Problems," *Flow, Its Measurement and Control in Science and Industry*, H. W. Stoll, ed., Instrument Soc. of Amer., p. 43 (1971).
Miiller, A., private communication (1999).
Nguyen, T. V., and I. L. Maclaine-Cross, "Incremental Pressure Drop Number in Parallel-Plate Heat Exchangers," *J. Fluids Eng.*, **110**, 93 (1988).
Ruegg, F. W., and H. H. Allion, "An Examination of the Effects of Heat Transfer and Compressible Flow on the Performance of Laminar Flowmeters," Fluid Meters Golden Anniversary Flow Measurement Conference, Pittsburgh, PA (1966). [Reprinted in *Precision Measurement and Calibration*, R. L. Bloss and M. J. Orloski, eds., National Bureau of Standards Special Publication 300, **8** (1972).]
Shapiro, A. H., *The Dynamics and Thermodynamics of Compressible Fluid Flow*, Ronald Press, New York (1953).
Strehlow, T., and E. Vogel, "Temperature Dependence and Initial Density Dependence of the Viscosity of Sulphur Hexafluoride," *Physica A*, **161**, 101 (1989).
Targett, M. J., W. B. Retallick, and S. W. Churchill, "Flow Through Curved Rectangular Channels of Large Aspect Ratio," *AIChE J.*, **41**, 1061 (1995).
Thomson, S. L., and W. R. Owens, "A Survey of Flows at Low Pressures," *Vacuum*, **25**, 151 (1975).
Tison, S. A., and L. Berndt, "High-Differential-Pressure Laminar Flowmeter," 1997 ASME Fluids Engineering Division Summer Meeting, Vancouver, BC, Canada (1997).
Van den Berg, H. R., C. A. ten Seldam, and P. S. van der Gulik, "Compressible Laminar Flow in a Capillary," *J. Fluid Mech.*, **246**, 1 (1993a).
Van den Berg, H. R., C. A. ten Seldam, and P. S. van der Gulik, "Thermal Effects in Compressible Viscous Flow in a Capillary," *Int. J. Thermophys.*, **14**, 865 (1993b).
Vogel, E., "Präzisionsmessungen des Viskositätskoeffizienten von Stickstoff und den Edelgasen zwischen Raumtemperatur und 650 K," *Ber. Bunsenges. Phys. Chem.*, **88**, 997 (1984).
Walowit, J., S. Tsao, and R. C. DiPrima, "Stability of Flow Between Arbitrarily Spaced Concentric Cylindrical Surfaces Including the Effect of a Radial Temperature Gradient," *J. Appl. Mech.*, **31**, 585 (1964).
White, C. M., "Streamline Flow through Curved Pipes," *Proc. Roy. Soc. Lond. A*, **123**, 645 (1929).

Appendix A: Derivation of the Flow Equation

We began by assuming that the differential pressure in the duct was the sum of a "Poiseuille" term and a "Bernoulli"

term. The corresponding differential equation is

$$-dP = \frac{3F_p\eta}{4ab^3}Qdz + \frac{\rho}{2}d\langle v^2\rangle, \quad \text{(A1)}$$

where $\langle v^2\rangle$ is the squared velocity averaged over the duct's cross section. After assuming an ideal-gas equation of state and integrating, we obtained

$$Q_1 = Q_0\left(\frac{1+y}{2}\right) + \frac{\rho_1 b}{10\eta aL}Q_1^2\ln(y), \quad \text{(A2)}$$

where Q_1 and ρ_1 are the volume flow rate and density at the duct's entrance, and $y \equiv P_2/P_1$. In the limit $y \to 1$, Q_1 approaches the volume flow rate Q_0 given by Eq. 3 for an *incompressible* fluid.

Similar derivations have been used to describe gas flow through capillary viscometers of circular cross section (Kawata et al., 1991). [Several derivations made the error of using $\langle v\rangle^2$ instead of $\langle v^2\rangle$ (van den Berg et al., 1993a).] Although the present derivation is less general than van den Berg et al.'s derivation of compressible flow through a duct of circular cross section (van den Berg et al., 1993a), the two have similar accuracy in the present range of density and Reynolds number.

The first term of Eq. A2 describes our data to within a few percent. Obtaining an accuracy of 0.1% requires inclusion of the second term to account for the acceleration caused by gas expansion along the duct. It also requires terms that account for entrance and expansion effects, slip, and departure of the gas's equation of state from that of an ideal gas. These terms use no free parameters and are discussed in the following subsections. Their derivations neglect the second term of Eq. A1.

Virial correction

We generalized the first term of Eq. A1 to a nonideal gas by making the substitution $Q = (\rho_1/\rho)Q_1$. We then used the pressure virial B_P to describe the gas's density as a function of the pressure P as

$$\rho = \frac{M}{RT}\frac{P}{(1+B_PP)}. \quad \text{(A3)}$$

Neglecting the Bernoulli term and integrating from the entrance to the exit, we obtained

$$\frac{M}{RT}\int_{P_1}^{P_2}\frac{PdP}{(1+B_PP)} = \frac{3\rho_1Q_1}{4F_pab^3}\int_0^L\eta(z)dz. \quad \text{(A4)}$$

Evaluation of the lefthand integral yields terms with factors such as $\ln(1+B_PP_1)$. Expanding these factors leads to the molar flow rate

$$\dot{n} = \frac{\rho_1Q_1}{M} = \frac{P_1Q_0}{RT}\left(\frac{1+y}{2}\right)[1+g_{\text{virial}}(B_PP_1,y)], \quad \text{(A5)}$$

where the virial correction function is

$$g_{\text{virial}}(B_PP_1,y) = -\frac{2(B_PP_1)}{3}\left(\frac{1-y^3}{1-y^2}\right) + \frac{(B_PP_1)^2}{2}\left(\frac{1-y^4}{1-y^2}\right) + O\left[(B_PP_1)^3\right], \quad \text{(A6)}$$

and the average viscosity is given by Eq. 5. The second term of g_{virial} was less than 0.001 for all of the present measurements except for SF_6 at the highest flow rates.

Expansion correction

The second term of Eq. A2 is small for the present impedance, which allows Q_1 in the second term to be approximated by the first term. Equation A2 then becomes

$$Q_1 = Q_0\left(\frac{1+y}{2}\right)\left[1+\frac{K_{\text{exp}}}{5}\frac{b}{L}Re\ln(y)\right], \quad \text{(A7)}$$

where $K_{\text{exp}} = 1$. The actual value of K_{exp} is larger because gas expansion distorts the velocity profile from the assumed parabolic form. To derive the value of K_{exp}, we approximated the flow as that between parallel plates ($b/a \to 0$). Appropriate modification of van den Berg et al.'s calculation for a circular cross section (van den Berg et al., 1993a) then yielded $K_{\text{exp}} = 9/7$.

Entrance correction

The increase in kinetic energy that occurs near the duct's entrance causes a pressure drop

$$\Delta P_1 = -K_{\text{ent}}\rho_1v_1^2 = -K_{\text{ent}}\rho_1[Q_1/(4ab)]^2, \quad \text{(A8)}$$

where $v_1 = Q_1/(4ab)$ is the average velocity at the duct's entrance. This correction is small for the present impedance because $\Delta P_1 \ll (P_1 - P_2)$. Therefore, we used the first term of Eq. A2 to approximate Q_1 in Eq. A8 and obtained

$$\frac{\Delta P_1}{P_1} \cong -\frac{K_{\text{ent}}}{12}\frac{b}{L}Re(1-y^2). \quad \text{(A9)}$$

Replacing P_1 in Eq. A9 by $P_1 - \Delta P_1$ leads to the volume flow rate

$$Q_1 = Q_0\left(\frac{1+y}{2}\right)\left[1-\frac{\Delta P_1}{P_1}\left(\frac{1+y^2}{1-y^2}\right)\right]. \quad \text{(A10)}$$

Inserting Eq. A9 into Eq. A10 yields the molar flow rate

$$\dot{n} = \frac{P_1(1-\Delta P_1/P_1)}{RT}Q_1 \quad \text{(A11)}$$

$$= \frac{P_1Q_0}{RT}\left(\frac{1+y}{2}\right)\left[1+\frac{K_{\text{ent}}}{6}\frac{b}{L}Re\right]. \quad \text{(A12)}$$

Our model used the value $K_{\text{ent}} = -0.9$ calculated at $Re = 200$ for a rectangular duct of narrow aspect ratio (Nguyen and Maclaine-Cross, 1988). The model assumed that K_{ent} was independent of Re at lower values of Re. This assumption caused little error, because the entrance correction was negli-

gible for $Re < 200$.

Slip correction

The correction for slip was similar to that used for circular capillaries (Thomson and Owens, 1975). The slip correction to the first term of Eq. A2 is

$$Q_1 = Q_0\left(\frac{1+y}{2}\right)\left[1+6K_{\text{slip}}\frac{\bar{\lambda}}{2b}\right], \tag{A13}$$

where

$$K_{\text{slip}} = \frac{2}{f_S} - 1. \tag{A14}$$

Due to the rectangular duct's narrow aspect ratio ($b/a \ll 1$), the slip correction's dependence on the channel width a is neglected. Although the accommodation coefficient f_S can depend on both the surface material and its thermal history (Dawe, 1970), its usual value is near $f_S = 1$ (Dittmann et al., 1989), corresponding to negligible specular reflection of molecules at the duct's walls. We therefore assigned $K_{\text{slip}} = 1$. Assuming $f_S < 1$ increased K_{slip} and caused negative deviations of the modeled flow at the lower flow rates.

Neglected corrections

We neglected flow near the duct's exit because the associated pressure drop $\Delta P_2 = K_{\text{exit}}\,\rho_2 v_2^2$ was expected to be negligible. Batchelor (1967) argues that, for liquid exiting a tube of radius R into a reservoir of radius R_{res}, $K_{\text{exit}} \approx (R/R_{\text{res}})^2$. A typical value for K_{exit} would thus be less than 0.01. See also the discussion in Section 3 of Kestin et al. (1973).

We neglected flow-induced deviations of the gas temperature from the temperature of the duct walls. Van den Berg et al. (1993b) estimated these deviations for a circular cross section and found that the difference between the radially averaged temperature $\langle T\rangle$ and the wall temperature T_0 is approximately

$$\langle T\rangle - T_0 \simeq -\frac{2}{3}\frac{\eta\langle v\rangle^2}{\kappa}, \tag{A15}$$

where η, κ, and $\langle v\rangle$ are the fluid's viscosity, thermal conductivity, and radially averaged velocity. (The flow causes the gas to cool by an amount that is independent of the duct's radius.) The largest such temperature difference was only 0.04 K and therefore negligible.

Table B1. Gas-Dependent Properties

Gas	M (kg·mol^{-1})	η_0 (μPa·s)	$(\partial\eta/\partial T)_\rho/\eta$ (K^{-1})	$(\partial\eta/\partial\rho)_T/\eta$ (m^3·kg^{-1})	B_P (Pa^{-1})
He	0.0040026	19.860	+0.00231	−0.00024	$+4.80\times10^{-9}$
N_2	0.028014	17.782	+0.00258	+0.00076	-2.02×10^{-9}
Ar	0.03995	22.599	+0.00283	+0.00055	-6.60×10^{-9}
SF_6	0.14605	15.234	+0.00296	−0.00001	-1.12×10^{-7}

Appendix B: Gas Properties

We used published values for the gas-dependent quantities used in the model. The model is most sensitive to the value of the low-density viscosity η_0 evaluated at 25.00°C and in the limit of zero pressure. Uncertainty in ratios of η_0 among the four gases is the largest contribution to the model's uncertainty because the duct height is an adjustable parameter in the model. To minimize uncertainty in the viscosity ratios, we used values of η_0 measured in one laboratory, that of Vogel and coworkers. Therefore, although the correlation of Bich et al. (1990) estimates the uncertainty of the viscosities of He and Ar as 0.3%, the uncertainty of the viscosity ratios is probably smaller.

For each measurement we estimated the average viscosity $\bar{\eta}$ as η_0, corrected by the temperature and the density $\rho(\bar{P})$ at the average pressure $\bar{P}$, according to

$$\bar{\eta} = \eta\left[T, \rho(\bar{P})\right] = \eta_0\left[1+\left(\frac{\partial\eta}{\partial T}\right)_\rho\frac{(T-T_0)}{\eta}+\left(\frac{\partial\eta}{\partial\rho}\right)_T\frac{\rho}{\eta}\right]. \tag{B1}$$

The density dependence of the viscosity of SF_6 happens to cross through zero near 25°C. Therefore, for SF_6 only, we added to Eq. B1 a quadratic term with the value $(\partial^2\eta/\partial\rho^2)[\rho^2/(2\eta_0)] = 8\times10^{-6}$ (ρ·kg^{-1}·m^3)^2 (Hoogland et al., 1985). The remaining gas properties are listed in Table B1. Values for M and B_P come from the Design Institute of Physical Property Data (DIPPR) database (1999), values for η_0 and $(\partial\eta/\partial T)_\rho/\eta$ come from Vogel (1984) and Strehlow and Vogel (1989), and values for $(\partial\eta/\partial\rho)_T/\eta$ come from Bich and Vogel (1996) and Strehlow and Vogel (1989).

Manuscript received Feb. 11, 2000, and revision received Aug. 21, 2000.